Fat-Suppression Techniques for 3-T MR Imaging of the Musculoskeletal System1

Filippo Del Grande, MD, MBA, MHEM, **Francesco Santini, PhD**, **Daniel A. Herzka, PhD**, **Michael R. Aro, MBBS**, **Cooper W. Dean, MD**, **Garry E. Gold, MD, MSEE**, and **John A. Carrino, MD, MPH**

Abstract

Fat suppression is an important technique in musculoskeletal imaging to improve the visibility of bone-marrow lesions; evaluate fat in soft-tissue masses; optimize the contrast-to-noise ratio in magnetic resonance (MR) arthrography; better define lesions after administration of contrast material; and avoid chemical shift artifacts, primarily at 3-T MR imaging. High-field-strength (eg, 3-T) MR imaging has specific technical characteristics compared with lower-field-strength MR imaging that influence the use and outcome of various fat-suppression techniques. The most commonly used fat-suppression techniques for musculoskeletal 3-T MR imaging include chemical shift (spectral) selective (CHESS) fat saturation, inversion recovery pulse sequences (eg, short inversion time inversion recovery [STIR]), hybrid pulse sequences with spectral and inversion-recovery (eg, spectral adiabatic inversion recovery and spectral attenuated inversion recovery [SPAIR]), spatial-spectral pulse sequences (ie, water excitation), and the Dixon techniques. Understanding the different fat-suppression options allows radiologists to adopt the most appropriate technique for their clinical practice.

Introduction

Fat-suppression techniques are an important part of musculoskeletal imaging. There are several key situations in which it is desirable to remove the fat contribution from the total magnetic resonance (MR) imaging signal with no or a minimal effect on the water signal. In general, fat-suppression techniques may be used to enhance contrast resolution and improve

the visibility of lesions to determine their lipid content and remove some artifacts. In musculoskeletal MR imaging, fat suppression is specifically used to improve depiction of bone-marrow edema (ie, lesions), confirm or exclude the presence of fat in soft-tissue tumors, differentiate high-signal-intensity structures on T1- and T2-weighted images (eg, protein-rich fluid and methemoglobin), eliminate chemical shift artifacts, better visualize enhancing lesions on T1-weighted gadolinium contrast material–enhanced images, and better differentiate tissues of interest (eg, cartilage, ligaments, and bone metastases) from surrounding fat (1–3).

High-field-strength (3-T) MR imaging is becoming more widely used for a variety of musculoskeletal applications, such as high-resolution imaging of small joints, hyaline cartilage, neoplasms, and peripheral nerves (neurography). Although these applications benefit from the improved image quality afforded by 3-T MR imaging, modifications in imaging strategies and protocols are required to effectively operate at this higher field strength, depending on the type of imaging needed. Most of the clinical applications for which 3-T MR imaging is used still exploit ^{1}H imaging, and the signal used to create images is induced by hydrogen nuclei. Compared with 1.5 T, 3-T MR imaging has several different properties related to its field strength, including T1 lengthening, higher signal-to-noise ratio (SNR), wider chemical shift between the fat- and water-signal peak, larger susceptibility effects with resultant artifacts, higher specific absorption rate (SAR), and greater B_0 and B_1 heterogeneity (4,5). These differences affect the reliability and consistency of fat suppression, require modifying certain pulse-sequence parameters, and, thus, alter the protocol choices used with musculoskeletal 3-T MR imaging in clinical practice.

In this article, we review the different options for fat suppression available with 3-T MR imaging with respect to their basis in physics; pulse-sequence design, with an emphasis on their strengths and limitations for musculoskeletal imaging; and any vendor-specific implementation strategies and nomenclature. The four 3-T MR imaging vendors are referred to in alphabetical order as follows: GE (General Electric Healthcare, Milwaukee, Wis); Philips (Philips Medical Systems, Best, the Netherlands); Siemens (Siemens Medical Solutions, Erlangen, Germany); and Toshiba (Toshiba Medical Systems, Tokyo, Japan). It should be noted that information about the vendors' implementation strategies and comparisons between vendors has been described as much as possible because such information is often considered proprietary and, therefore, is not available.

Physics

Because of their spin properties, hydrogen nuclei in water and fat molecules are the main contributors to MR signal. The two hydrogen nuclei in water molecules provide the same contribution to the signal, whereas in adipose tissue, many hydrogen nuclei in different chemical environments contribute to the signal. The remaining hydrogen nuclei in the body (ie, outside the water and fat) are not significantly involved in signal generation because they either decay too rapidly (eg, protons in macromolecules) or have only a small relative abundance with respect to fat and water, making them undetectable with nonspectroscopic methods (eg, metabolites) (6). To generate an MR signal in which the fat contribution is minimized and the water contribution is not substantially affected, the two main differences

in the MR properties of fat and water—precessional (Larmor) frequencies and T1 relaxation times—may be exploited.

Precessional Frequencies

The different precessional frequencies of fat and water are a result of the greater electronic shielding of the protons in fat molecules compared with water molecules. The protons in fat molecules precess at a slightly lower frequency than the protons in water (2). This difference in frequency is also known as chemical shift, which is linearly proportional to the external magnetic field B_0, as shown in Equation 1:

$$C_s = \frac{\gamma}{2\pi} B_0 \Delta \partial \, [ppm] \, 10^{-6}, \quad \text{(1)}$$

where

$$\frac{\gamma}{2\pi}$$

is the gyromagnetic ratio in Hz/T (42.6 Mhz/T) (2).

It is also possible to exploit this effect for chemical shift–based fat-suppression techniques, such as chemical shift–selective (ie, spectral) fat suppression (CHESS), spatial-spectral sequences, and Dixon (fat-water separation) techniques. Compared with a weaker magnetic field, the wider chemical shift separation between water and fat that occurs at 3-T allows for more selective fat saturation, which is limited only by the higher B_0 and B_1 heterogeneity of 3-T MR imaging. The main fat peak has a resonance frequency 420 Hz lower than that of water at 3 T, compared with 210 Hz lower at 1.5 T and 145 Hz lower at 1.0 T.

T1 Relaxation Time

T1 relaxation time, also called longitudinal relaxation time and spin-lattice relaxation, is the time constant by which protons restore their longitudinal magnetization toward the equilibrium state after the excitation of the radiofrequency (RF) pulse. T1 relaxation time is a characteristic of each tissue and is longer with stronger magnetic fields (7–10). Fat has a shorter T1 relaxation time than water and is approximately 288 msec at 1.5 T and 371 msec at 3 T (8). T1 relaxation time is the basic principle of inversion-based fat-suppression techniques.

Pulse Sequences

In general, to suppress the fat-signal contribution for any given MR imaging sequence, a fat-suppression module is inserted into the sequence, usually at the beginning or as a replacement for the excitation pulse, or, with Dixon techniques, at the time of signal acquisition after the excitation pulse. A variety of fat-suppression techniques may be used to capitalize on the available MR imaging properties to minimize the fat-signal contribution. The main categories (families) of fat-suppression pulse sequences are CHESS, short inversion time inversion recovery (STIR), hybrid techniques, water excitation, and Dixon techniques (Fig 1).

Chemical Shift– selective Fat Suppression

Physics Basis

In 1985, Haase et al (11) described a CHESS sequence that may be used to obtain either pure water or pure fat images on the basis of the chemical shift difference between water and fat. For fat suppression, an excitation pulse with a narrow bandwidth centered on the resonance frequency of fat (chemically selective RF pulse) and a flip angle of 90° tips the magnetic vector of fat in the transverse plane. This process is immediately followed by a "homogeneity" spoiler gradient that is applied to dephase the protons and, thus, suppress the fat signal (11,12). Images are acquired as soon as the dephasing gradient is finished and before the recovery time of longitudinal magnetization for fat begins (Fig 2a) (2). The distance between the water peak and the fat peak increases with the magnetic field strength, a trait that is beneficial for more selective fat suppression at 3 T compared with a weaker magnetic field. In fact, on MR images obtained with a weaker magnetic field, the two peaks tend to overlap, which may lead to heterogeneous fat suppression (6).

Clinical Considerations

CHESS is a technique that is commonly used in musculoskeletal MR imaging to suppress fat in a number of joints, such as the knee, hand, and wrist. It is also used in MR arthrography because of its selectivity for fat, high SNR, and relatively fast examination time. Compared with inversion-recovery techniques, the fat selectivity of CHESS is crucial to optimize visualization of lesions on contrast material–enhanced T1-weighted images and tissue characterization. However, CHESS is B_0- and B_1-sensitive, a characteristic that may produce heterogeneity in fat suppression (1).

Fat-suppression techniques that are based on chemical shift fat selection tend to work better at higher magnetic field strengths, presuming B_0 and B_1 homogeneity. B_0 heterogeneity may shift the water and main fat peaks so that the fat-saturation RF pulse falls outside the fat frequency range (2). A large field of view, off-center imaging, and anatomic regions with challenging geometric features (eg, the neck) are less suitable for CHESS because of their higher B_0 heterogeneity (Figs 3, 4). Because of the increased number of susceptibility artifacts, CHESS is not suitable for patients with metallic implants and should be avoided for evaluation of arthroplasty and other postoperative conditions in which substantial amounts of metal are present (Table 1).

B_1 heterogeneity is another limitation of chemical fat suppression. To achieve homogeneous fat saturation, the saturation of the fat peak requires a well-defined flip angle (FA), with an acceptable variation range of 5°–10°. FAs that fall outside this range will only partially saturate the fat (2). To achieve effective fat suppression, the RF pulse must excite spin only in fat molecules. The central frequency of the RF pulse should be 420 Hz lower than that of water, and the frequency range should be carefully selected so that only spins of fat molecules are excited. The frequency range is called the spectral bandwidth. Spectral bandwidth is a different concept than readout bandwidth and increases, along with the central frequency, as magnetic field strength increases. Furthermore, with conventional RF pulses, the homogeneity of fat suppression is rendered sensitive to variations of the FA in

different spatial locations inside the body (6). The flip angle of conventional RF pulses is proportional to the amplitude of the B_1 field, which is then modulated by the electric characteristics of the tissue. This drawback may be overcome by using so-called adiabatic RF pulses, which are special pulses that sweep a range of frequencies and are largely insensitive to the absolute amplitude of the RF field. These pulses are usually longer and are used, for example, in the SPAIR technique.

Because of the wider chemical shift at high-field-strength MR imaging, the use of spectral fat suppression yields better results at 3 T than at 1.5 T near the isocenter, with a good RF coil to mitigate the B_0 and B_1 sensitivities. It is important to mention that doubling of the susceptibility artifacts at 3 T is not strong enough to nullify the benefit of wider chemical shift. Therefore, at higher magnetic fields, better fat suppression may be achieved with a wider bandwidth in the fat frequency range and a shorter RF pulse (2,13).

Vendor-specific Implementations

Three MR imaging vendors—GE, Siemens, and Toshiba—offer pure CHESS fat suppression with a presaturation pulse and without inversion time, whereas Philips uses a hybrid sequence with a spectrally selective inversion pulse known as spectral presaturation with inversion recovery (SPIR). Toshiba uses the multisection off-resonance fat-suppression technique (MSOFT) to suppress the fat signals on a section-by-section basis rather than applying a global CHESS pulse. The section-selective nature of MSOFT produces uniform fat suppression by adapting to magnetic field differences, which typically worsen as a function of distance from the isocenter, and provides more homogeneous fat suppression in body parts that are not easily positioned near the isocenter, such as the shoulder, elbow, and wrist (Table 2) (Fig 5a, 5b).

STIR Pulse Sequences

Physics Basis

The technique for STIR pulse sequences was first introduced by Bydder et al (9,10) as a variant of the previously used inversion-recovery sequences at low-field-strength MR imaging. Inversion-recovery techniques are based on the T1 relaxation time of the tissues being imaged (9,10,14,15). After applying a 180° inversion pulse, the longitudinal magnetization of fat recovers faster than that of water and crosses the zero line (no net magnetization) after an inversion time (TI) = $T_1 \log 2$. The application of a 90° excitation pulse at the time the fat signal crosses the null line produces a fat-free signal (16). However, because water has a longer T1 relaxation time, it takes longer to reach the null line, and it still produces a reduced signal. The time between the 180° inversion pulse and the 90° acquisition pulse is the TI (Fig 2b) (1). Because of its longer T1 recovery time, the TI of 3-T MR imaging needed to nullify the fat signal is in the range of 205–225 msec compared with 100–200 msec for 1.5 T (2). By modulating TI, it is possible to adjust the strength of the fat suppression desired: a TI that is close to the exact nulling time will have the strongest fat suppression, whereas a lower or higher TI will have weaker fat suppression (Fig 6a, 6b).

Clinical Considerations

STIR is insensitive to B_0 and B_1 heterogeneity. Thus, STIR sequences are widely used in musculoskeletal imaging because of the improved fat suppression that may be achieved in off-center imaging (eg, the elbow, hand, and wrist, with the patient lying supine and the arm positioned along the body), in the presence of metal (eg, postoperative arthroplasty), with a large field of view (eg, the entire spine in the setting of spondyloarthritis or metastatic neoplasm), and in challenging anatomic regions with multiple airtissue interfaces (eg, the brachial plexus, fingers, and toes). The presence of metallic implants has only a minimal impact on the homogeneity of fat suppression (Fig 7a, 7b).

The major clinical limitations of STIR sequences are their relatively long imaging times, low SNR, and high SAR. Long imaging times may be reduced by using a rapid acquisition with relaxation enhancement (RARE), such as a fast or turbo spin-echo pulse-sequence technique. Low SNR is a major drawback in applications, such as the wrist and foot and MR neurography, that require a high SNR. SNR may be improved with use of a shorter TE, although this technique reduces the T2 weighting of the sequence. Furthermore, STIR is not a fat-specific suppression technique because a TI that suppresses fat signal has the same effect on other tissues and substances with a short T1 relaxation time, such as methemoglobin, mucoid tissue, proteinaceous material, and melanin (17). Similarly, gadolinium contrast material shortens the T1 relaxation time of enhanced tissues, and, for the same reason, gadolinium-containing intraarticular fluid may be suppressed by the inversion pulse. Therefore, STIR sequences are not suitable for contrast material–enhanced imaging or MR arthrography (Table 1) (1). STIR is available from all four 3-T MR imaging vendors (GE, Philips, Siemens, and Toshiba), with no substantial differences in implementation (Table 2).

Hybrid Techniques

Physics Basis

Hybrid techniques for fat suppression are a combination of CHESS and inversion-recovery sequences. A spectrally selective inversion pulse is applied to flip the fat spins by 180°. After an inversion (recovery) time (TI), a conventional excitation pulse is applied; this technique is known as SPIR. Specifically designed adiabatic pulses may be introduced to deal with RF spatial nonuniformity (B_1 heterogeneity). Adiabatic pulses achieve inversion of the magnetization not by applying electromagnetic power at a single frequency, but by sweeping through a frequency range. This technique makes the FA relatively independent of the absolute pulse amplitude (provided that it is above a certain threshold) and dependent on the frequency evolution of the pulse and is known as SPAIR (Fig 2c) (18).

SPIR is a hybrid fat-suppression technique that combines the fat selectivity of CHESS and the inversion RF pulse of STIR. SPIR differs from CHESS in that its RF pulse is an inversion pulse, and it differs from STIR in that its inversion pulse is selective for excitation of fat spins only. There is no difference in the TI needed to suppress fat between the two techniques. The advantages of SPIR are that it has a higher SNR than does STIR and it does not suppress other tissues with a T1 relaxation time similar to that of fat. However, SPIR is

B_0- and B_1-sensitive, requires a good separation between fat and water peaks to achieve effective fat suppression, and requires a longer run time than when fat suppression is not used (6).

Clinical Considerations

The SPAIR pulse sequence has two main advantages: As was previously mentioned, because of its adiabatic pulse, it is relatively insensitive to B1 heterogeneity compared with CHESS, and it has a higher SNR than does STIR. A SPIR-SPAIR hybrid fat suppression technique has a higher SNR than STIR because the inversion pulse of the SPIR-SPAIR hybrid is fat selective, whereas that of STIR is not. At the time of fat T1 recovery, other tissue types do not have enough time for T1 recovery; therefore, the SNR for those tissues is lower. By contrast, SPAIR employs composite RF pulses to spectrally separate fat and water through dephasing, with a small delay between short RF pulses. Therefore, SPAIR does not have the same loss of SNR from inversion recovery and is a good technique to use when homogeneous and SNR-efficient fat suppression is needed over a large field of view, such as in the thighs and thoraco-abdominopelvic regions (Figs 8, 9). Lauenstein et al (19) reported that the use of SPAIR resulted in a lower SNR (ie, superior fat suppression) for mesenteric and retroperitoneal fat than did inversion recovery, a finding that is particularly important in musculoskeletal imaging, tumor imaging, and MR neurography (20–22).

A disadvantage of hybrid sequences is that, because of their B_0 sensitivity, they may show heterogeneous fat suppression, mainly at the edges of short MR bores when the field of view is larger than the shimmed area. To minimize this problem, it is possible to use a Dixon technique to obtain more homogeneous, SNR-efficient fat suppression or to acquire two sets of images and then merge the acquisitions. STIR is another option that provides homogeneous fat suppression with lower SNR (Table 1) (Fig 10). Further disadvantages of hybrid sequences are a longer pulse duration and higher SAR.

Vendor-specific Implementation

Spectral inversion at lipid (SPECIAL) is a non-adiabatic sequence that uses a spectral selective inversion pulse and is available on GE equipment. SPAIR sequences are available on Philips, Siemens, and Toshiba equipment, whereas SPIR sequences are available only on Philips equipment. SPIR is often used as a hybrid between inversion recovery and fat saturation, with flip angles of around 110°, and is followed by dephasing gradients (23). Most of the fat signal is excited and subsequently disrupted, as in conventional fat saturation, whereas the inversion component of the pulse compensates for T1 recovery between the SPIR pulse and the excitation (Table 2).

Water Excitation

Physics Basis

Water excitation is a "spatial-spectral" pulse sequence that was originally designed by Meyer and colleagues (24) to simultaneously select a spatial band (section thickness) and a spectral band (water), which excites the water inside a section and leaves the fat and all spins outside the section unaltered. Water excitation is accomplished by using a binomial RF

pulse, which is actually a set of RF pulses with a double net effect (ie, a 90° pulse for water spins and a 0° pulse for fat spins) (6). In the simplest form of water excitation (called a 1–1 pulse), an RF pulse with a flip angle equal to one-half the desired flip angle is initially applied to both water and fat (25). Then, the fat and water begin to lose phase coherence. When they both precess 180° out of phase (about 1 msec at 3 T and about 2 msec at 1.5 T and calculated with the formula

$$\Delta T = \frac{1}{2\Delta f},$$

where f is the frequency shift between water and fat), another RF pulse is applied to flip the fat back to the longitudinal axis, and the water experiences another excitation that is summed to the previous one (Fig 2d). Other schemes with more than two pulses or phase advances of less than 180° are also possible, but, in general, the longer the excitation scheme, the more insensitive the technique is to B_0 heterogeneities.

Clinical Considerations

The water-excitation technique is relatively fast because there is no need for a spoiler gradient to delay relaxation (6). It also has relatively high SNR and insensitivity to B_1 heterogeneity. Water excitation techniques are widely used to evaluate cartilage because of their fast imaging time and high SNR and contrast-to-noise ratio (CNR). In clinical practice, water excitation techniques are generally applied to gradient-echo sequences, but they are also used with turbo spin-echo (TSE), fast spin-echo (FSE), and spin-echo (SE) sequences, as is detailed in the "Vendor-specific Implementation" section. The ideal FA setting for a double-echo steady-state (DESS) sequence with water excitation at 3 T has been reported to be 20° for maximum cartilage signal and 90° for maximum synovial signal, which provide the highest CNR between cartilage and synovial fluid. At 1.5 T, these values are 30° and 90°, respectively (26). Hauger and colleagues (27) applied water-excitation fat suppression to three commonly used SE and FSE sequences (contrast-enhanced T1-weighted SE, intermediate-weighted FSE, and T2-weighted FSE) and compared them with CHESS fat suppression in various joints of 83 patients. The authors found that water excitation was faster and produced images with higher SNR and CNR (for images obtained with intermediate-weighted sequences) than did CHESS. At 3 T, water excitation benefits from wider spectral separation between water and fat and shorter spaces between RF pulses than at lower field strengths; however, this shorter spacing also requires shorter RF pulses and stronger gradients, which increase SAR (Table 1) (2).

Vendor-specific Implementation

Spectral-spatial (GE, Milwaukee, Wis), ProSet (Philips, Best, the Netherlands), water excitation (Siemens, Erlangen, Germany), and the water excitation technique (WET; Toshiba, Tokyo, Japan) are similar water-excitation sequences. We are not aware of any clinically relevant differences between the vendors, except in the type of sequences that may be used with water-excitation techniques. The GE spectral-spatial technique must be run with gradient-echo sequences, such as coherent oscillatory state acquisition for the manipulation of image contrast (COSMIC), whereas Philips has no restriction with SE or

TSE sequences (Fig 11). Similar to GE, the Siemens technique allows water excitation to be used only in gradient-echo sequences, such as DESS, volumetric interpolated brain examination (VIBE), and fast imaging with steady-state precession (FISP) sequences and not in TSE sequences (Fig 12). The Siemens equipment also allows for "fast" or "normal" water-excitation schemes with different pulse schemes; the "normal" scheme is more robust to B_0 heterogeneity but slower than the "fast" version. WET may be used with gradient-echo sequences and SE or FSE sequences. Polarity-altered spectral and spatial selective acquisition (PASTA; Toshiba, Tokyo, Japan) is different than WET in that the excitation pulse is so narrow as to excite only water. Because PASTA includes a 180° pulse, it may be used only with SE-based sequences (Table 2).

Dixon Techniques

Physics Basis

The chemical shift–based fat-water separation method was described by Dixon in 1984 (28) as a two-point method. Now, various techniques exist that are commonly referred to as the Dixon techniques. Two-point Dixon techniques acquire either two different images or two images with two different TEs in each image to decompose the fat signal from the water signal in the same voxel (6). Because the water and fat spins precess at different frequencies, their magnetization vectors rotate with respect to each other between excitation and acquisition, becoming alternatively "in phase" (ie, pointing in the same direction) and "out of phase" (ie, pointing in opposite directions). Because the acquired signal is proportional to the vector sum of the magnetizations when the spins are in phase, the total signal is proportional to the sum of the magnitude; when the spins are out of phase, the signal is proportional to the difference.

One image is obtained with the fat and water spins in phase (signal in-phase [SIP]), and one image is obtained with the spins out of phase (signal out-of-phase [SOP]). At 1.5 T, the difference in echo time (TE) between the two states is about 2.2 msec (out-of-phase TEs: 2.2 msec, 6.6 msec, etc.; in-phase TEs: 4.4 msec, 8.8 msec, etc). At 3 T, the difference in TEs is about 1.1 msec (29). Pure water images are obtained by adding the SIP to the SOP (Eq 2), and pure fat images are obtained by subtracting the SOP from the SIP (Eq 3).

$$W = \frac{SIP + SOP}{2}. \quad (2)$$

$$F = \frac{SIP - SOP}{2}. \quad (3)$$

Thus, it is possible to obtain a pure water image with fat suppression and a pure fat image with water suppression (2). This technique is insensitive to B_1 heterogeneity and may be used with several sequences, such as T1- and T2-weighted FSE, gradient-echo, and steady-state free precession (SSFP) imaging (Fig 2e) (2).

Two-point Dixon techniques may be limited by B_0 heterogeneity, which may shift fat and water peaks and suppress the unwanted component (eg, fat instead of water), an effect called

fat-water swapping that may be avoided by using unwrapping algorithms that compensate for the B_0 field heterogeneity (Fig 13). Several modifications followed the original two-point Dixon methods. The first was proposed by Glover and Schneider (30) and added a third image to compensate for the B_0 sensitivity of the original two-point Dixon method. The authors called this modified technique the three-point Dixon method and used a three-phase difference of 0, π, and $-\pi$ between the fat and water signals (30). Later, Glover (31) proposed an extension of the three-point Dixon method called the four-point Dixon method, which used four images with phase differences of 0, π, 2π, and 3π. Three- and four-point Dixon techniques are more robust to field heterogeneity than two-point Dixon methods, but they have longer examination times and lower SNR efficiency (SNR per unit time). Over the next few years, several modifications of the original Dixon technique were developed, with several application schemes and algorithms; however, detailed descriptions of these modifications are beyond the scope of this article.

Clinical Considerations

Because it is insensitive to B_0 and B_1 heterogeneity, the Dixon technique offers robust and SNR-efficient fat suppression, even in areas with high magnetic susceptibility (eg, metallic implants), in anatomic regions that are difficult to image, and in the extremities in pediatric and elderly patients who cannot tolerate uncomfortable positions (Figs 14–16) (32,33). In two different studies, fast three-point Dixon techniques were compared with T2-weighted CHESS fat suppression in pediatric imaging of the musculoskeletal system and spine at 1.5 T MR imaging in clinical practice (34,35). In both studies, the fast three-point Dixon technique led to more homogeneous and robust fat suppression in the extremities and spine, particularly in the hands and feet among pediatric patients, whereas CHESS was more prone to field heterogeneity. In both studies, lesion visibility was significantly better with the fast three-point Dixon method than with CHESS; thus, fast three-point Dixon techniques may be used in musculoskeletal imaging as an alternative to T2-weighted CHESS fat suppression. When a large field of view—such as the abdomen, spine, and pelvis—is used, fat-suppression techniques often have problems with heterogeneous fat suppression (eg, CHESS fat suppression) because of B_0 heterogeneity or ineffective fat suppression (eg, STIR sequences). The use of Dixon techniques may help minimize these limitations (Table 1) (36).

The original Dixon technique was a relatively long sequence because it acquired multiple images at fixed TEs. The development of several reconstruction algorithms made it shorter and more suitable for clinical practice. Furthermore, the time savings that may be achieved with the use of parallel imaging make it a good addition to the Dixon technique at high magnetic field strengths. The higher SNR of 3 T with the higher SNR of the Dixon technique may easily offset the decreased SNR of parallel imaging, making it possible to obtain SNR-efficient homogeneous fat suppression in clinical practice (37,38).

Another important advantage of the Dixon technique is the potential for absolute quantification of the percentage of fat in each voxel, a feature that may result in some interesting applications in musculoskeletal imaging. MR spectroscopy may be used to differentiate between extra- and intramyocellular lipid on the basis of the frequency

difference between them and could be important in identifying insulin resistance that may be treated with diet and exercise (39–43). Another interesting application is monitoring of the fat and water levels in red bone marrow during therapy for hematologic disease; however, to date, several problems—such as different T1 weighting of the fat and water signals, T2* decay, and complex decay of fat due to its multipeak spectrum—limit accurate quantification of fat at MR imaging (2,44–46). Therefore, the development of a fat quantification algorithm will be an important topic in the near future. Similar to the water excitation method, the precession frequency increases at higher field strengths, making the echo spacing required for a specific phase offset between water and fat shorter and, thus, enabling faster acquisitions.

Vendor-specific Implementation

Although the principles for fat-water separation all derive from the original work of Dixon more than 2 decades ago, the 3-T MR imaging vendors have several different strategies for applying fat-water separation techniques, including the use of reconstruction algorithms to decrease sequence time, avoid fat-water swapping, and increase homogeneity (28). The iterative decomposition of water and fat with echo asymmetry and least-squares estimation (IDEAL; GE, Milwaukee, Wis) is a fat-water separation technique used by GE and based on a three-point Dixon method with a bespoke reconstruction algorithm (Fig 17) (32,47). IDEAL is widely used in general musculoskeletal imaging and allows robust fat suppression in body areas with challenging anatomy, such as the fingers and neck (48–52). Flex (GE; Milwaukee, Wis), a two-point technique also offered by GE, is another option for fat-water separation (Fig 18). FLEX is faster (two acquisitions instead of three) and is usually used in areas where speed is important, such as in dynamic contrast imaging or in patients who are more prone to move during the examination, but its fat suppression is lower than that achieved with IDEAL. Multipoint Dixon (M Dixon; Philips, Best, the Netherlands) may be used as a two-, three-, or four-point Dixon technique with a different reconstruction algorithm. It is mainly used in abdominal imaging but is applicable for musculoskeletal imaging as well (Fig 19). Siemens has a two- and three-point Dixon method that may be used with several musculoskeletal applications, and Toshiba has a dual-echo sequence that allows for in-phase and out-of-phase visualization (Table 2).

Summary

It is important that radiologists and technologists be aware of the advantages and disadvantages of the various fat suppression techniques available for musculoskeletal 3-T MR imaging in order to select the most appropriate technique for a particular situation in clinical practice. In particular, STIR is a robust fat suppression technique at every field strength, including 3 T, but it may have low SNR. CHESS has higher SNR than STIR, but it is limited by field heterogeneity at 3 T. Hybrid (spectral and inversion-recovery) sequences and Dixon techniques offer SNR-efficient and robust fat suppression that, when combined with parallel imaging, could play a central role in 3-T musculoskeletal imaging in the future. Water excitation takes advantage of the wider spectral fat-water separation in these hybrid sequences and will likely be an important technique for cartilage imaging because of its

relatively fast acquisition times and high CNR. In addition to several advantages, every technique also presents some challenges that should be considered in clinical practice.

Acknowledgments

Abbreviations

CHESS	chemical shift–selective fat suppression
CNR	contrast-to-noise ratio
FA	flip angle
FSE	fast spin echo
RF	radiofrequency
SAR	specific absorption rate
SE	spin echo
SNR	signal-to-noise ratio
SPAIR	spectral adiabatic inversion recovery
SPIR	spectral presaturation with inversion recovery
STIR	short inversion time inversion recovery
TE	echo time
3D	three-dimensional
TI	inversion time
TR	repetition time
TSE	turbo spin echo

References

1. Delfaut EM, Beltran J, Johnson G, Rousseau J, Marchandise X, Cotten A. Fat suppression in MR imaging: techniques and pitfalls. RadioGraphics. 1999; 19(2):373–382. [PubMed: 10194785]

2. Bley TA, Wieben O, François CJ, Brittain JH, Reeder SB. Fat and water magnetic resonance imaging. J Magn Reson Imaging. 2010; 31(1):4–18. [PubMed: 20027567]

3. Aoki T, Yamashita Y, Oki H, et al. Iterative decomposition of water and fat with echo asymmetry and least-squares estimation (IDEAL) of the wrist and finger at 3T: comparison with chemical shift selective fat suppression images. J Magn Reson Imaging. 2013; 37(3):733–738. [PubMed: 22911970]

4. Gold GE, Suh B, Sawyer-Glover A, Beaulieu C. Musculoskeletal MRI at 3.0 T: initial clinical experience. AJR Am J Roentgenol. 2004; 183(5):1479–1486. [PubMed: 15505324]

5. Kuo R, Panchal M, Tanenbaum L, Crues JV 3rd. 3.0 Tesla imaging of the musculoskeletal system. J Magn Reson Imaging. 2007; 25(2):245–261. [PubMed: 17260407]

6. Cameron, I. Techniques of Fat Suppression. http://cds.ismrm.org/protected/09MProceedings/files/Tues%20C36_01%20Cameron.pdf. Accessed April 29, 2013

7. Duewell SH, Ceckler TL, Ong K, et al. Musculoskeletal MR imaging at 4 T and at 1.5 T: comparison of relaxation times and image contrast. Radiology. 1995; 196(2):551–555. [PubMed: 7617876]

8. Gold GE, Han E, Stainsby J, Wright G, Brittain J, Beaulieu C. Musculoskeletal MRI at 3.0 T: relaxation times and image contrast. AJR Am J Roentgenol. 2004; 183(2):343–351. [PubMed: 15269023]

9. Bydder GM, Pennock JM, Steiner RE, Khenia S, Payne JA, Young IR. The short TI inversion recovery sequence: an approach to MR imaging of the abdomen. Magn Reson Imaging. 1985; 3(3): 251–254. [PubMed: 4079672]

10. Bydder GM, Young IR. Clinical use of the partial saturation and saturation recovery sequences in MR imaging. J Comput Assist Tomogr. 1985; 9(6):1020–1032. [PubMed: 4056131]

11. Haase A, Frahm J, Hänicke W, Matthaei D. 1H NMR chemical shift selective (CHESS) imaging. Phys Med Biol. 1985; 30(4):341–344. [PubMed: 4001160]

12. Keller PJ, Hunter WW Jr, Schmalbrock P. Multisection fat-water imaging with chemical shift selective presaturation. Radiology. 1987; 164(2):539–541. [PubMed: 3602398]

13. Bernstein, MA.; King, KF.; Zhou, XJ. Handbook of MRI pulse sequences. Elsevier; Burlington, Mass: 2004. Spectral radiofrequency pulses; p. 115-124.

14. Smith RC, Constable RT, Reinhold C, McCauley T, Lange RC, McCarthy S. Fast spin echo STIR imaging. J Comput Assist Tomogr. 1994; 18(2):209–213. [PubMed: 8126269]

15. Atlas SW, Grossman RI, Hackney DB, Goldberg HI, Bilaniuk LT, Zimmerman RA. STIR MR imaging of the orbit. AJR Am J Roentgenol. 1988; 151(5):1025–1030. [PubMed: 3263000]

16. Bernstein, MA.; King, KF.; Zhou, XJ. Handbook of MRI pulse sequences. Elsevier; Burlington, Mass: 2004. Basic pulse sequences; p. 622-624.

17. Krinsky G, Rofsky NM, Weinreb JC. Nonspecificity of short inversion time inversion recovery (STIR) as a technique of fat suppression: pitfalls in image interpretation. AJR Am J Roentgenol. 1996; 166(3):523–526. [PubMed: 8623620]

18. Bernstein, MA.; King, KF.; Zhou, XJ. Handbook of MRI pulse sequences. Elsevier; Burlington, Mass: 2004. Adiabatic radiofrequency pulses; p. 190-198.

19. Lauenstein TC, Sharma P, Hughes T, Heberlein K, Tudorascu D, Martin DR. Evaluation of optimized inversion-recovery fat-suppression techniques for T2-weighted abdominal MR imaging. J Magn Reson Imaging. 2008; 27(6):1448–1454. [PubMed: 18504735]

20. Chhabra A, Andreisek G, Soldatos T, et al. MR neurography: past, present, and future. AJR Am J Roentgenol. 2011; 197(3):583–591. [PubMed: 21862800]

21. Chhabra A, Lee PP, Bizzell C, Soldatos T. 3 Tesla MR neurography: technique, interpretation, and pitfalls. Skeletal Radiol. 2011; 40(10):1249–1260. [PubMed: 21547613]

22. Chhabra A, Faridian-Aragh N. High-resolution 3-T MR neurography of femoral neuropathy. AJR Am J Roentgenol. 2012; 198(1):3–10. [PubMed: 22194473]

23. Kaldoudi E, Williams SC, Barker GJ, Tofts PS. A chemical shift selective inversion recovery sequence for fat-suppressed MRI: theory and experimental validation. Magn Reson Imaging. 1993; 11(3):341–355. [PubMed: 8505868]

24. Meyer CH, Pauly JM, Macovski A, Nishimura DG. Simultaneous spatial and spectral selective excitation. Magn Reson Med. 1990; 15(2):287–304. [PubMed: 2392053]

25. Bernstein, MA.; King, KF.; Zhou, XJ. Handbook of MRI pulse sequences. Elsevier; Burlington, Mass: 2004. Spatial radio-frequency pulses; p. 153-163.

26. Moriya S, Miki Y, Matsuno Y, Okada M. Three-dimensional double-echo steady-state (3D-DESS) magnetic resonance imaging of the knee: establishment of flip angles for evaluation of cartilage at 1.5 T and 3.0 T. Acta Radiol. 2012; 53(7):790–794. [PubMed: 22850576]

27. Hauger O, Dumont E, Chateil JF, Moinard M, Diard F. Water excitation as an alternative to fat saturation in MR imaging: preliminary results in musculoskeletal imaging. Radiology. 2002; 224(3):657–663. [PubMed: 12202695]

28. Dixon WT. Simple proton spectroscopic imaging. Radiology. 1984; 153(1):189–194. [PubMed: 6089263]

29. Schindera ST, Soher BJ, Delong DM, Dale BM, Merkle EM. Effect of echo time pair selection on quantitative analysis for adrenal tumor characterization with in-phase and opposed-phase MR imaging: initial experience. Radiology. 2008; 248(1):140–147. [PubMed: 18566172]

30. Glover GH, Schneider E. Three-point Dixon technique for true water/fat decomposition with B0 inhomogeneity correction. Magn Reson Med. 1991; 18(2):371–383. [PubMed: 2046518]

31. Glover GH. Multipoint Dixon technique for water and fat proton and susceptibility imaging. J Magn Reson Imaging. 1991; 1(5):521–530. [PubMed: 1790376]

32. Reeder SB, Wen Z, Yu H, et al. Multicoil Dixon chemical species separation with an iterative least-squares estimation method. Magn Reson Med. 2004; 51(1):35–45. [PubMed: 14705043]

33. Yu H, Reeder SB, Shimakawa A, Brittain JH, Pelc NJ. Field map estimation with a region growing scheme for iterative 3-point water-fat decomposition. Magn Reson Med. 2005; 54(4):1032–1039. [PubMed: 16142718]

34. Rybicki FJ, Chung T, Reid J, Jaramillo D, Mulkern RV, Ma J. Fast three-point Dixon MR imaging using low-resolution images for phase correction: a comparison with chemical shift selective fat suppression for pediatric musculoskeletal imaging. AJR Am J Roentgenol. 2001; 177(5):1019–1023. [PubMed: 11641161]

35. Ma J, Singh SK, Kumar AJ, Leeds NE, Zhan J. T2-weighted spine imaging with a fast three-point Dixon technique: comparison with chemical shift selective fat suppression. J Magn Reson Imaging. 2004; 20(6):1025–1029. [PubMed: 15558561]

36. Hu HH, Börnert P, Hernando D, et al. ISMRM workshop on fat-water separation: insights, applications and progress in MRI. Magn Reson Med. 2012; 68(2):378–388. [PubMed: 22693111]

37. Pruessmann KP, Weiger M, Scheidegger MB, Boesiger P. SENSE: sensitivity encoding for fast MRI. Magn Reson Med. 1999; 42(5):952–962. [PubMed: 10542355]

38. Sodickson DK, Manning WJ. Simultaneous acquisition of spatial harmonics (SMASH): fast imaging with radiofrequency coil arrays. Magn Reson Med. 1997; 38(4):591–603. [PubMed: 9324327]

39. Schick F, Eismann B, Jung WI, Bongers H, Bunse M, Lutz O. Comparison of localized proton NMR signals of skeletal muscle and fat tissue in vivo: two lipid compartments in muscle tissue. Magn Reson Med. 1993; 29(2):158–167. [PubMed: 8429779]

40. Boesch C, Slotboom J, Hoppeler H, Kreis R. In vivo determination of intra-myocellular lipids in human muscle by means of localized 1H-MR-spectroscopy. Magn Reson Med. 1997; 37(4):484–493. [PubMed: 9094069]

41. Szczepaniak LS, Dobbins RL, Stein DT, McGarry JD. Bulk magnetic susceptibility effects on the assessment of intra- and extramyocellular lipids in vivo. Magn Reson Med. 2002; 47(3):607–610. [PubMed: 11870849]

42. Krssak M, Falk Petersen K, Dresner A, et al. Intra-myocellular lipid concentrations are correlated with insulin sensitivity in humans: a 1H NMR spectroscopy study. Diabetologia. 1999; 42(1):113–116. [PubMed: 10027589]

43. Jacob S, Machann J, Rett K, et al. Association of increased intramyocellular lipid content with insulin resistance in lean nondiabetic offspring of type 2 diabetic subjects. Diabetes. 1999; 48(5):1113–1119. [PubMed: 10331418]

44. Machann J, Pereira PL, Einsele H, Kanz L, Claussen CD, Schick F. The MR characterization of the composition of the hematopoietic bone marrow: the findings in generalized neoplasms and the monitoring of therapy [in German]. Radiologe. 2000; 40(8):700–709. [PubMed: 11006940]

45. Schick F, Weiss B, Einsele H. Magnetic resonance imaging reveals a markedly inhomogeneous distribution of marrow cellularity in a patient with myelodysplasia. Ann Hematol. 1995; 71(3):143–146. [PubMed: 7548333]

46. Schick F, Einsele H, Lutz O, Claussen CD. Lipid selective MR imaging and localized 1H spectroscopy of bone marrow during therapy of leukemia. Anticancer Res. 1996; 16(3B):1545–1551. [PubMed: 8694524]

47. Reeder SB, Pineda AR, Wen Z, et al. Iterative decomposition of water and fat with echo asymmetry and least-squares estimation (IDEAL): application with fast spin-echo imaging. Magn Reson Med. 2005; 54(3):636–644. [PubMed: 16092103]

48. Reeder SB, Yu H, Johnson JW, et al. T1- and T2-weighted fast spin-echo imaging of the brachial plexus and cervical spine with IDEAL water-fat separation. J Magn Reson Imaging. 2006; 24(4): 825–832. [PubMed: 16969792]

49. Gold GE, Reeder SB, Yu H, et al. Articular cartilage of the knee: rapid three-dimensional MR imaging at 3.0 T with IDEAL balanced steady-state free precession—initial experience. Radiology. 2006; 240(2):546–551. [PubMed: 16801369]

50. Gerdes CM, Kijowski R, Reeder SB. IDEAL imaging of the musculoskeletal system: robust water fat separation for uniform fat suppression, marrow evaluation, and cartilage imaging. AJR Am J Roentgenol. 2007; 189(5):W284–W291. [PubMed: 17954627]

51. Kijowski R, Blankenbaker DG, Woods MA, Shinki K, De Smet AA, Reeder SB. 3.0-T evaluation of knee cartilage by using three-dimensional IDEAL GRASS imaging: comparison with fast spin-echo imaging. Radiology. 2010; 255(1):117–127. [PubMed: 20173102]

52. Blankenbaker DG, Ullrick SR, Kijowski R, et al. MR arthrography of the hip: comparison of IDEAL-SPGR volume sequence to standard MR sequences in the detection and grading of cartilage lesions. Radiology. 2011; 261(3):863–871. [PubMed: 21900621]

ONLINE-ONLY SA-CME LEARNING OBJECTIVES

After completing this journal-based SA-CME activity, participants will be able to:

■Describe the physics underlying the various mechanisms of fat suppression for 3-T MR imaging.

■Discuss the advantages and disadvantages of the different methods of fat-suppression for MR imaging of the musculoskeletal system.

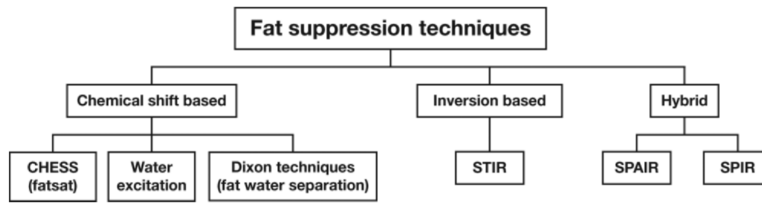■List the vendor-specific implementation strategies, pulse sequence names, and parameters currently available for 3-T MR imaging.

Figure 1.

Chart shows the major types of fat suppression—chemical shift–based, inversion-based, and hybrid—used in 3-T musculoskeletal MR imaging.
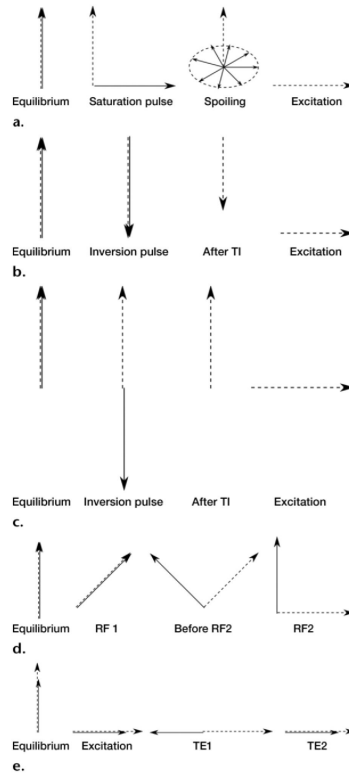
Figure 2.
Fat suppression techniques. Dashed arrow = water, solid arrow = fat. **(a)** Diagram shows the mechanism of CHESS fat suppression, in which fat is selectively excited by an RF pulse, and a gradient pulse is applied to disperse the magnetization in the transverse plane. **(b)** Diagram shows the mechanism of coronal STIR fat suppression, in which the fat signal is inverted with a non-selective 180° pulse, and acquisition is begun after the inversion time *(TI)* that nulls the fat signal, resulting in a water signal with reduced magnitude. **(c)** Diagram shows the mechanism of spectral adiabatic inversion-recovery (SPAIR) fat suppression, in which the fat signal is inverted with an adiabatic spectrally selective pulse, and acquisition is begun after the inversion time that nulls the fat signal. **(d)** Diagram shows the mechanism of water excitation, in which an excitation pulse with an FA that equals one-half the desired FA is applied, and a delay is introduced to allow the water and fat magnetization to fall out of phase. At this point, a second excitation pulse is applied, which brings the fat magnetization back to the longitudinal axis and finishes flipping the water magnetization onto the transverse plane. **(e)** Diagram shows the mechanism of the Dixon technique, in which both water and fat are excited, and the first echo *(TE1)* is acquired when the two magnetization vectors in the transverse plane are out of phase, creating destructive interference. The second echo *(TE2)* is acquired when the two vectors are in phase, creating constructive addition.
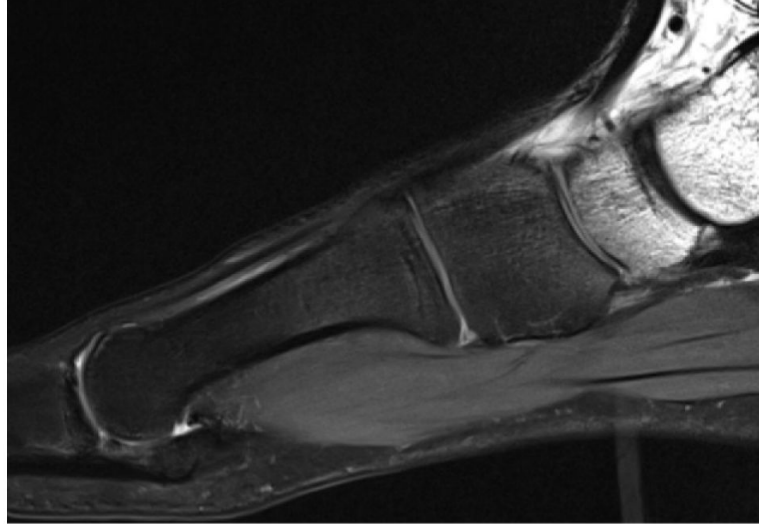
Figure 3.
Sagittal T2-weighted MR image (repetition time [TR], 3000 msec; echo time [TE], 44 msec) of the foot shows heterogeneous fat suppression with CHESS fat saturation, a result of the challenging anatomic geometry.
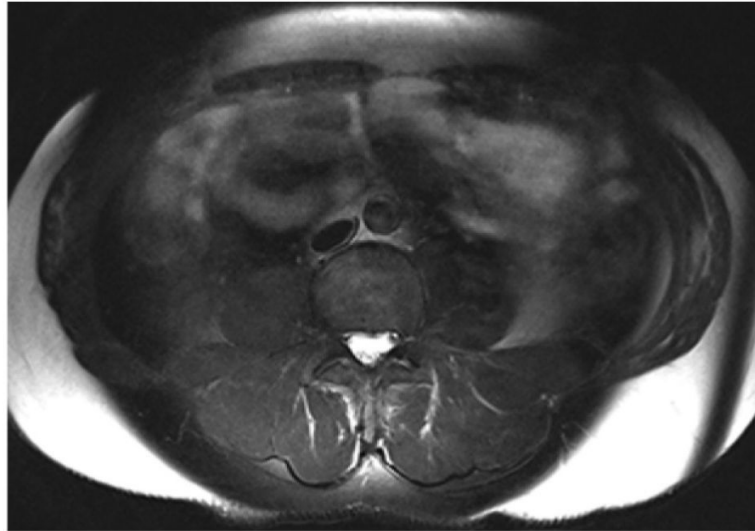
Figure 4.
Axial T2-weighted CHESS MR image (TR, 4590 msec; TE, 75 msec) of the abdomen shows that subcutaneous fat was not suppressed, a result of strong B0 inhomogeneity in a large field of view.
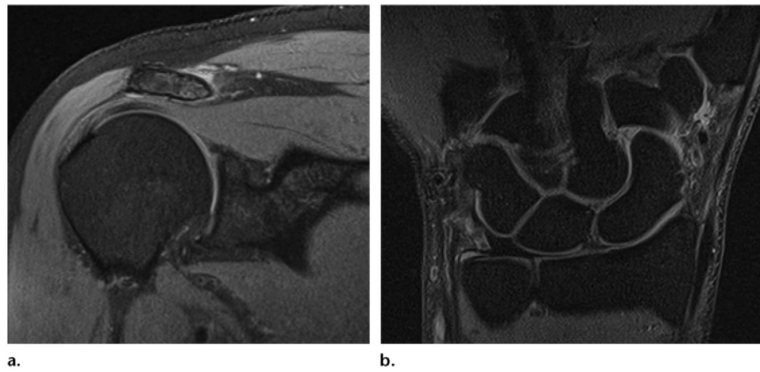
Figure 5.
Multisection off-resonance fat-suppression technique (MSOFT). Coronal unenhanced fat-saturated proton density–weighted MR images of a normal right shoulder (TR, 3000 msec; TE, 24 msec; FA, 90°) **(a)** and a normal right wrist (TR, 2150 msec; TE, 18 msec; FA, 90°) **(b)** show the effects of MSOFT.
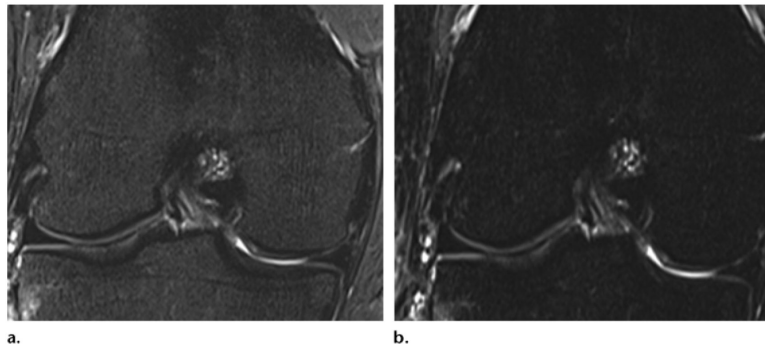
Figure 6.
Effects of STIR imaging in the knee. **(a)** STIR MR image (TR, 4500 msec; TE, 27 msec; TI, 205 msec) shows weak fat suppression of bone marrow. **(b)** STIR MR image (TR, 4500 msec; TE, 27 msec; TI, 220 msec) shows stronger fat suppression. (Images courtesy of Rory Johnson, RT, Siemens Medical Solutions, and Peter Cazares, Senior MR Education Specialist, Siemens Medical Solutions.)
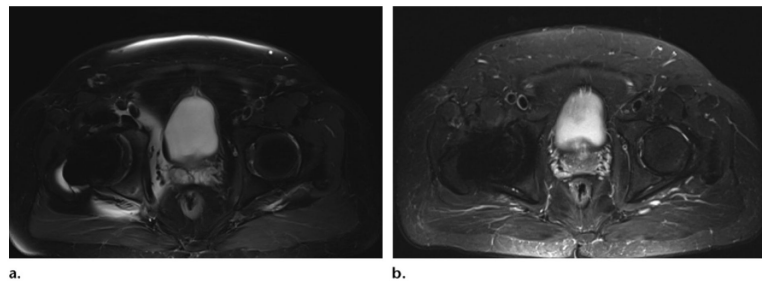
Figure 7.
Axial T2-weighted SPAIR fat-suppressed (TR, 4000 msec; TE, 74 msec) **(a)** and STIR (TR, 3970 msec; TE, 54 msec; TI, 220 msec) **(b)** MR images show that susceptibility artifacts from metal hip implants are more pronounced on SPAIR images, which are B_0 sensitive, than they are on STIR images, which are not.
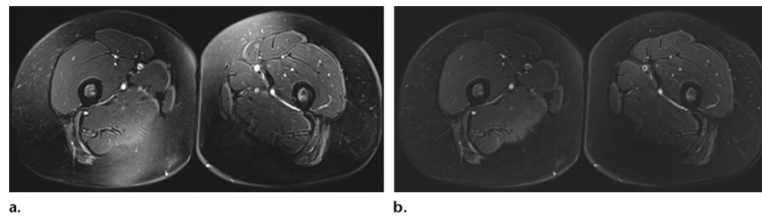
Figure 8.
(a) Axial T2-weighted CHESS MR image (TR, 5550 msec; TE, 10 msec) shows heterogeneity of the fat suppression signal in the posteromedial aspect of the right thigh and the anteromedial aspect of the left thigh. **(b)** Axial T2-weighted SPAIR MR image (TR, 5550 msec; TE, 10 msec) shows more homogeneous fat suppression.
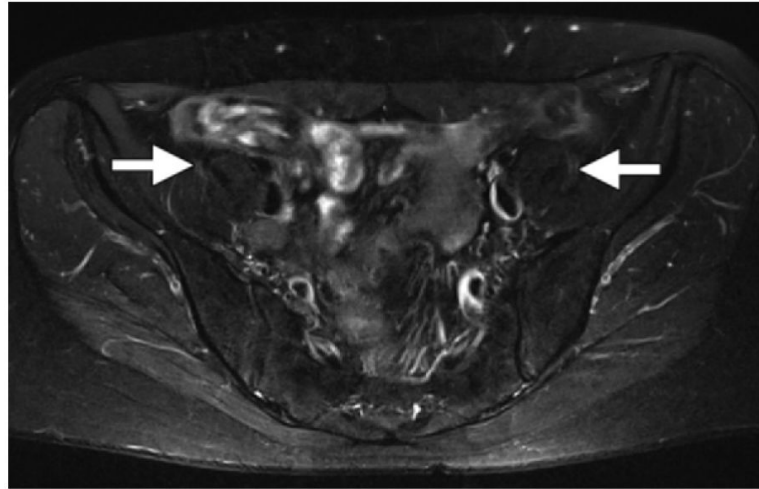
Figure 9.
Axial T2-weighted (TR, 5000 msec; TE, 80 msec) SPAIR MR neurographic image of the pelvis shows homogeneous, SNR-efficient fat suppression and normal femoral nerves (arrows), which are slightly hyperintense.
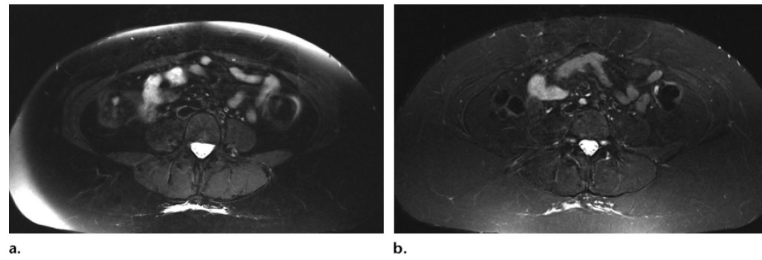
Figure 10.
(a) Axial T2-weighted SPAIR MR image (TR, 4590 msec; TE, 75 msec) shows heterogeneous suppression of subcutaneous fat, a result of B_0 inhomogeneity at the edge of the large field of view. **(b)** STIR MR image (TR, 3960 msec; TE, 47 msec; TI, 220 msec) shows homogeneous suppression of subcutaneous fat.
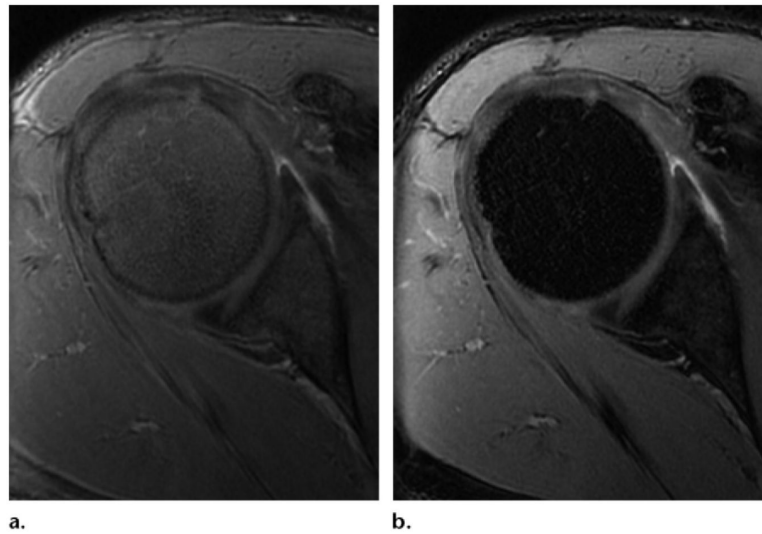
Figure 11.
Comparison of coherent oscillatory state acquisition for the manipulation of image contrast (COSMIC) and SPECIAL sequences. Three-dimensional (3D) COSMIC (GE, Milwaukee, Wis) MR image of the shoulder with chemical fat saturation (TR, 5.3 msec; TE, 1.5 msec; FA, 45°) **(a)** and SPECIAL (GE, Milwaukee, Wis) MR image with fat saturation (TR, 5.5 msec; TE, 1.3 msec; FA, 45°) **(b)** show stronger fat saturation with the SPECIAL technique.
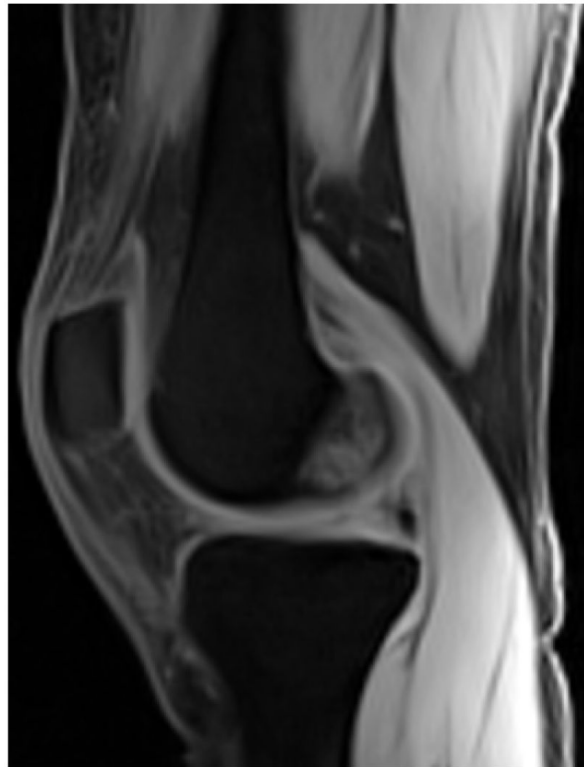
Figure 12.
Water excitation technique. Sagittal VIBE (Siemens, Erlangen, Germany) MR image (TR, 20 msec; TE, 2.8 msec; FA, 15°) obtained with the water excitation technique shows a normal knee.
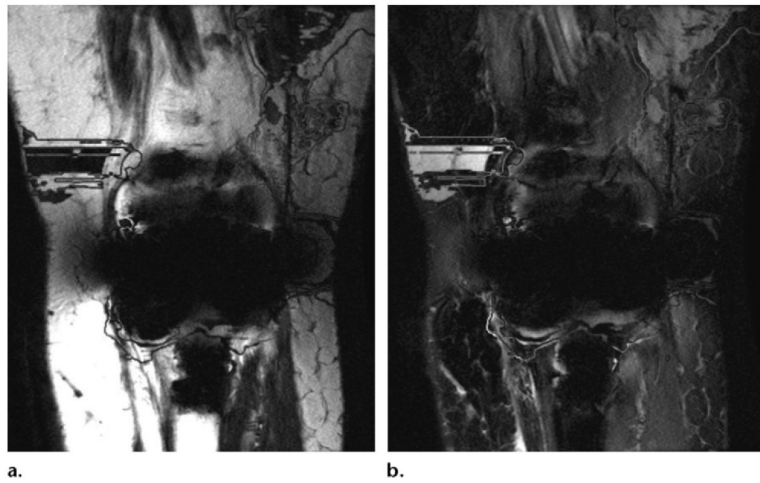
Figure 13.
Fat-water swapping in a patient with total knee replacement. Iterative decomposition of water and fat with echo asymmetry and least-squares estimation (IDEAL; GE, Milwaukee, Wis) MR images (TR, 3000 msec; TE, 13 msec) with fat **(a)** and water **(b)** only show severe field heterogeneity and fat-water swapping.
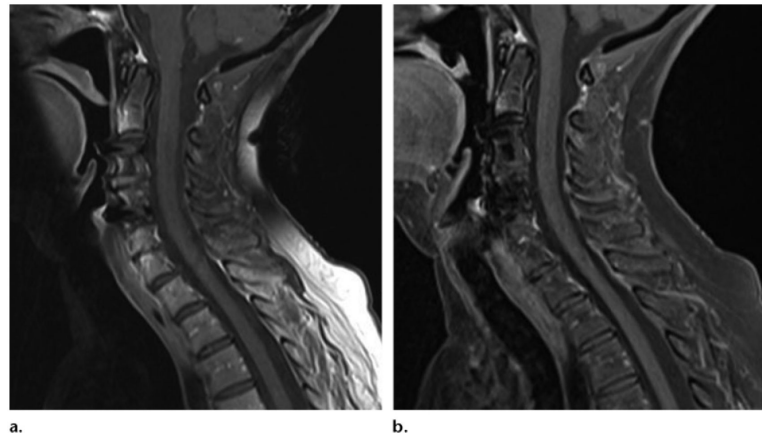
Figure 14.
(a) Sagittal T1-weighted MR image with chemical fat saturation (TR, 500 msec; TE, 10 msec) shows heterogeneous fat saturation of the subcutaneous fat in the posterior side of the neck. **(b)** Dixon (Siemens, Erlangen, Germany) MR image (TR, 610 msec; TE, 12 msec) of the cervical spine shows robust fat suppression. (Images courtesy of Rory Johnson and Peter Cazares.)
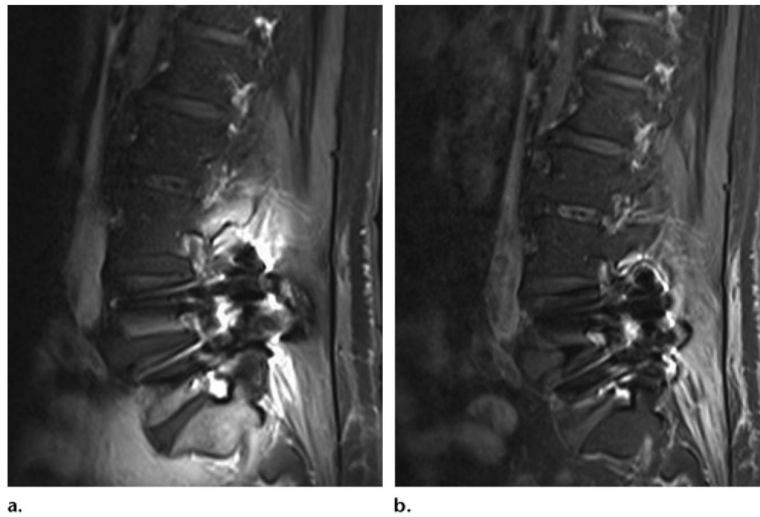
Figure 15.
Sagittal T1-weighted MR image with chemical fat saturation (TR, 510 msec; TE, 10 msec) **(a)** and Dixon (Siemens) MR image (TR, 692 msec; TE, 12 msec) **(b)** of the lumbar spine obtained in a patient with metal artifacts show that susceptibility artifacts are significantly greater with CHESS than fat-water separation. (Images courtesy of Rory Johnson and Peter Cazares.)
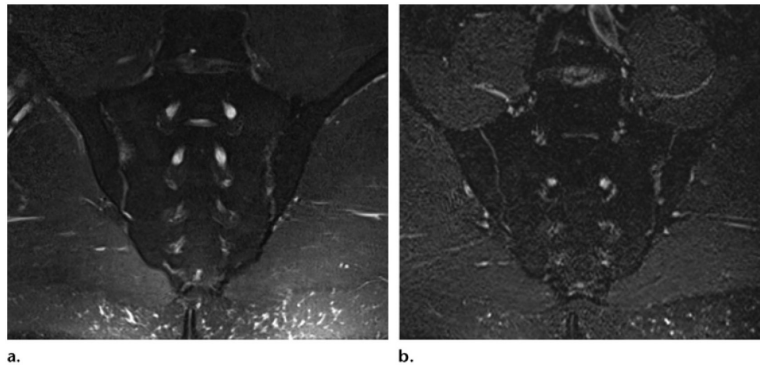
Figure 16.
Coronal Dixon (Siemens) (TR, 3500 msec; TE, 90 msec) **(a)** and 3D SPACE STIR (TR, 5040 msec; TE, 47 msec; TI, 220 msec) **(b)** MR images of the sacrum show that SNR is lower with STIR than it is with fat-water separation. (Images courtesy of Rory Johnson and Peter Cazares.)

Figure 17.
(a–c) Sagittal in-phase **(a)**, fat **(b)**, and water **(c)** IDEAL (GE) MR images (TR, 3800 msec; TE, 28 msec) obtained in a patient who underwent anterior cruciate ligament reconstruction show a fluid collection near the interference screw (arrow in **c**), with no artifacts. **(d)** Sagittal proton density–weighted MR image with chemical fat saturation (TR, 4000 msec; TE, 32 msec) shows unsuppressed fat near the screw (arrow).

Figure 18.
Three-dimensional (3D) maximum intensity projection Cube Flex (GE, Milwaukee, Wis)
MR neurogram of the lumbar plexus (TR, 1800 msec; TE, 35 msec) shows fat-water
separation and FSE contrast. Cube Flex uses a 3D FSE acquisition and a two-point fat-water
separation method to obtain high-resolution 3D images.

Figure 19.
Multipoint (four-point) high-resolution 3D ($0.5 \times 0.5 \times 1.5$ mm^3) Dixon (Philips, Best, the Netherlands) MR images (TR, 10.4 msec) obtained in phase **(a)**, out of phase **(b)**, with water suppression **(c)**, and with fat only **(d)** show a normal knee.

Table 1

Advantages and Disadvantages of Different Fat-Suppression Techniques in Musculoskeletal MR Imaging

Technique	Imaging Time	SNR	SAR	Effect of Metal	B$_0$ Sensitivity	B$_1$ Sensitivity	Preferred Field Strength
Chemical fat saturation	Short[*]	High	Medium	Strong	Sensitive	Sensitive	High
STIR	Long	Low	High	Minimal	Insensitive	Insensitive	Indifferent
SPIR	Long	High	High	Strong	Sensitive	Sensitive	High
SPAIR	Long	High	High	Strong	Sensitive	Insensitive	High
Water excitation	Short	High	Low	Strong	Sensitive	Insensitive	Medium[†]
Dixon	Long	High	Low	Mini-malw	Insensitive (three- or four-point Dixon)	Insensitive	Medium[†]

Source.—Reference 2.

Note.—All other MR imaging parameters should be considered equal. SPIR = spectral presaturation with inversion recovery.

[*] Depends on the pulse sequence.

[†] There are advantages and disadvantages at both high and low magnetic field strengths.

Table 2

Vendor-specific Fat-Suppression Techniques Available for 3-T MR Imaging Systems

	Vendor			
Sequence	GE	Philips	Siemens	Toshiba
CHESS	Fat saturation, chemical fat saturation	None	Fat saturation	Fat saturation
STIR	STIR	STIR	STIR	STIR
Hybrid spectral and inversion recovery	SPECIAL	SPIR (without adiabatic pulse)	SPAIR (with adiabatic pulse)	SPAIR
		SPAIR (with adiabatic pulse)		
Water excitation	Spectral spatial	ProSet	Water excitation	WET, PASTA
Dixon (fat-water separation)	IDEAL[*], Flex	mDixon	Dixon	WFOP

Note.—IDEAL = iterative decomposition of water and fat with echo asymmetry and least-squares estimation, mDixon = multi-point Dixon, PASTA = polarity-altered spectral and spatial selective acquisition, SPECIAL = spectral inversion at lipid, WET = water excitation technique, WFOP = water-fat opposed phase.

[*] Also known as the three-point fat-water separation technique.